The Astrophysical Journal, 709:358–368, 2010 January 20 doi:10.1088/0004-637X/709/1/358

SUZAKU BROADBAND SPECTROSCOPY OF *SWIFT* J1753.5−0127 IN THE LOW-HARD STATE

Mark T. Reynolds[1], Jon M. Miller[1], Jeroen Homan[2], and Giovanni Miniutti[3]
[1] Department of Astronomy, University of Michigan, 500 Church Street, Ann Arbor, MI 48109, USA; markrey@umich.edu
[2] MIT Kavli Institute for Astrophysics and Space Research, 70 Vasser Street, Cambridge, MA 02139, USA
[3] LAEX, Centro de Astrobiologia (CSIC–INTA); LAEFF, P.O. Box 78, E–28691, Villanueva de la Cañada, Madrid, Spain
Received 2009 January 24; accepted 2009 November 19; published 2009 December 31

ABSTRACT

We present *Suzaku* observations of the Galactic black hole candidate *Swift* J1753.5−0127 in the low-hard state (LHS). The broadband coverage of Suzaku enables us to detect the source over the energy range 0.6–250 keV. The broadband spectrum (2–250 keV) is found to be consistent with a simple power-law ($\Gamma \sim 1.63$). In agreement with previous observations of this system, a significant excess of soft X-ray flux is detected consistent with the presence of a cool accretion disk. Estimates of the disk inner radius infer a value consistent with the innermost stable circular orbit (ISCO; $R_{\rm in} \lesssim 6R_g$, for certain values of, e.g., $N_{\rm H}$, i), although we cannot conclusively rule out the presence of an accretion disk truncated at larger radii ($R_{\rm in} \sim 10$–$50R_g$). A weak, relativistically broadened iron line is also detected, in addition to disk reflection at higher energy. However, the iron-K line profile favors an inner radius larger than the ISCO ($R_{\rm in} \sim 10$–$20R_g$). The implications of these observations for models of the accretion flow in the LHS are discussed.

Key words: accretion, accretion disks – black hole physics – X-rays: binaries – X-rays: individual (*Swift* J1753.5−1027)

Online-only material: color figures

1. INTRODUCTION

The study of accretion processes is of fundamental astrophysical importance, being ubiquitous on both the largest and smallest scales, i.e., ranging from accretion by supermassive black holes in the center of galaxies at one end to star and planet formation at the other. Here we are interested in studying accretion phenomena in the presence of a large gravitational potential such as that observed in X-ray binaries (XRBs) and active galactic nuclei (AGNs). In these sources, the fundamental timescales of interest, governing the accretion process, scale with the mass of the central object ($\propto M_x$). Hence, studies of the Galactic XRB population provide an excellent laboratory for detailed examination of the process of accretion on humanly accessible timescales.

The very-high, high-soft, and low-hard states (hereafter VHS, HSS, and LHS) are the primary active accretion states observed in XRBs (see the review by McClintock & Remillard 2006 for a detailed description of accretion states in black hole binaries). Despite being the most common mode of accretion in black hole X-ray binaries, the nature of the accretion flow in the LHS remains uncertain. Emission in the LHS is characterized by a hard power-law spectrum ($\Gamma \sim 1.4$–1.7) and strong X-ray variability (30%–40% RMS). Correlated variability at radio/NIR/optical wavelengths has also been observed from the black hole systems while in the hard state (Fender 2006). The hard power-law component may be the result of Comptonization by a hot optically thin plasma of soft seed photons from a thermal disk or magnetic structures (through cyclo-synchrotron processes—see, e.g., Merloni et al. 2000). However, the geometry of this plasma is not well understood. A popular model for the accretion geometry in the LHS was given by Esin et al. (1997). In that model, the standard thin accretion disk that dominates in the spectrally soft states is radially truncated and replaced by an advection dominated accretion flow (ADAF; see Narayan et al. 2008). The fundamental assumption of a radially recessed accretion disk may find some support in the low disk reflection fractions which are sometimes measured in the hard state (e.g., Gierlinski et al. 1997).

A number of models have been developed which do not require a recessed disk in the LHS. Beloborodov (1999) proposed that black hole states are driven by the height and bulk velocity of magnetic flares above a disk, which remains at the innermost stable circular orbit (ISCO). These flares would serve to feed a mildly relativistically outflowing corona. Low disk reflection fractions do not signal a recessed disk in this model, but result from mild beaming of the hard X-ray flux away from the disk. A similar model for the LHS, based on magnetically dominated coronae, has been proposed by Merloni & Fabian (2002). These outflowing coronae share some properties with jet-based models for the hard component (Markoff et al. 2005) in the sense that the latter also produce low reflection fractions (Markoff & Nowak 2004) without the need for a recessed accretion disk.

A number of recent observations call into question the assumption of a recessed disk in the LHS. In particular, GX 339−4 was observed during its 2004 outburst at a luminosity of $L \sim 0.05L_{\rm Edd}$ by both the *Rossi X-Ray Timing Explorer* (*RXTE*) and *XMM-Newton* (Miller et al. 2006b). The observations by *XMM-Newton* are critical here as they provide coverage at energies below 3 keV, whereas *RXTE* is limited to energies above this. It was found that a cool disk blackbody (∼0.35 keV) consistent with an optically thick geometrically thin accretion disk extending to the ISCO existed, in contrast to theoretical expectations. Fits with reflection models revealed reflection fractions ∼0.2–0.3. Previous observations of *Swift* J1753.5−0127 yielded similar results for the cool disk component; in this case, a disk temperature of ∼0.2 keV was required by Miller et al. (2006a); however, no significant disk reflection features were detected.

Swift J1753.5−0127 was discovered by the *Swift* burst alert telescope (BAT) at X-ray and γ-ray energies on 2005 May 30

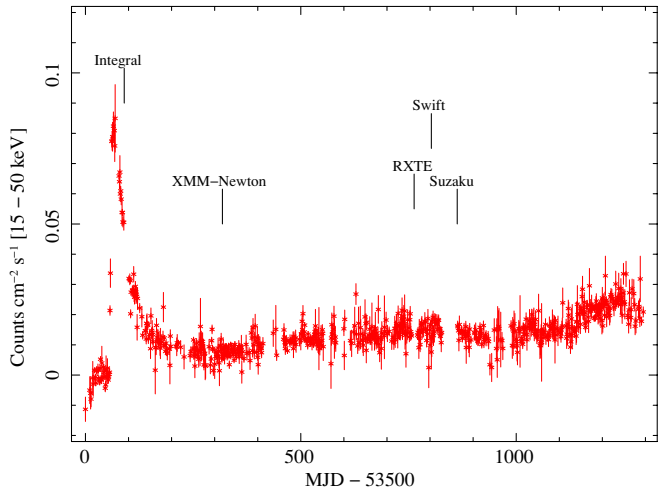

Figure 1. *Swift* BAT hard X-ray light curve for *Swift* J1753.5−0127 from 2005 May to 2008 November. The times of the *INTEGRAL* (Cadolle Bel et al. 2007), *XMM-Newton* (Miller et al. 2006a), *RXTE* (Durant et al. 2009), *Swift* (see Section 4.1), and *Suzaku* (this paper) observations are indicted.

(A color version of this figure is available in the online journal.)

(Palmer et al. 2005). Subsequent observations with the X-ray telescope (XRT) revealed a hard power-law spectrum (Burrows et al. 2005; Morris et al. 2005), while pointed *RXTE* observations detected 0.6 Hz quasi-periodic oscillations (QPO; Morgan et al. 2005). The system was also detected at UV (Still et al. 2005) and optical wavelengths (Halpern 2005). Radio observations with the MERLIN array also detected a variable counterpart (Fender et al. 2005). Observations at optical wavelengths by Zurita et al. (2008) have also detected a significant modulation with a period of 3.2 hr, which they identify as a superhump period slightly larger than the actual orbital period. This would make *Swift* J1753.5−0127 the black hole binary with the shortest known orbital period.

In addition to the observations of Miller et al. (2006a) above, a number of other high-energy studies of this source have been published, which we summarize below (see Figure 1). An analysis of *RXTE* observations of the outburst was reported in Zhang et al. (2007) and Ramadevi et al. (2007). The X-ray spectrum was found to be consistent with a power-law ($1.6 \leqslant \Gamma \leqslant 1.8$), while low-frequency QPOs were also detected (up to 0.9 Hz). Cadolle Bel et al. (2007) analyzed simultaneous *RXTE* and *International Gamma-Ray Astrophysics Laboratory* (*INTEGRAL*) data, which were also obtained during the 2005 outburst. The combined spectrum (3–400 keV) could be fit with a model consisting of thermal Comptonization modified by disk reflection ($kT_0 \sim 0.5$ keV, $kT_e \sim 150$ keV, $\tau \sim 1$, $f \equiv \Omega/2\pi \sim 0.3$). QPOs were also detected here, but at a lower frequency than during the outburst peak (0.24 Hz).

To place meaningful constraints on the accretion flow in the LHS, one requires sensitivity to both the soft X-rays (<2 keV) in order to detect the cool accretion disk and higher energies in order to detect the most prominent disk reflection features (5–7 keV and 20–30 keV). *Suzaku* with its large bandpass and low background is ideally equipped to carry out these observations. In this paper, we describe observations undertaken with the *Suzaku* X-ray observatory in 2007, while *Swift* J1753.5−0127 was in the LHS. In Section 2, we describe our observation and extraction of source spectra and light curves. We proceed to analyze the data in Section 3, where both phenomenological and more physically motivated models are considered. The broadband spectrum (2–250 keV) is consistent with a simple power-law model, although there are also contributions from the accretion disk. In Section 4, these results are discussed in the context of models for the accretion flow in the LHS, and finally our conclusions are presented in Section 5.

2. OBSERVATIONS

Swift J1753.5−0127 was observed while still in the LHS by *Suzaku* (Mitsuda et al. 2007) from 2007 September 19 20:36 UT until September 22 10:30 UT (obsid:402088010, PI: Homan; see Figure 1). Data were acquired over a broad spectral range (0.2–600 keV), with the X-ray imaging spectrometer (XIS; Koyama et al. 2007) and the hard X-ray detector (HXD; Takahashi et al. 2007; Kokubun et al. 2007). The source was observed at the XIS nominal position for total uncorrected exposure times of ∼95 ks and 82 ks, respectively.

All data reduction and analysis take place within the HEASOFT 6.4.1 environment, which includes FTOOLS 6.4, SUZAKU 8.0, and XSPEC 12.4.0x. The latest versions of the relevant *Suzaku* CALDB files were also used.

2.1. X-ray Imaging Spectrometer

The XIS is installed at the focal plane of the four X-ray telescopes (XRT; Serlemitsos et al. 2007) and currently consists of three functioning detectors XIS0, XIS1, and XIS3. XIS0 and XIS3 are front illuminated and provide coverage over the energy range 0.4–12 keV, whereas XIS1 is back illuminated in an effort to provide greater sensitivity at lower energies, 0.2–12 keV. The XIS has a field of view of ∼18′ × 18′ (1024^2 pixels) and was operated in 5×5, 3×3 readout mode. In addition, the data were taken in 1/4 window mode in an effort to minimize possible photon pileup, giving a time resolution of 2 s.

As the downloaded data products had been processed via the *Suzaku* pipeline v2.1.6.15, the data were reprocessed from the raw telemetry files as recommended in the *Suzaku* data reduction guide (abc guide).[4] Standard screening was applied, in particular, we extracted *ASCA* event grades 0:0, 2:4, 6:6 with the data filtered to be taken outside of the South Atlantic Anomaly (SAA) and where the earth elevation angle was greater than 5°. Good time interval (GTI) events were extracted using XSELECT, where the 3×3 and 5×5 observation mode data for each detector were extracted simultaneously. Science images, spectra, and backgrounds were then extracted from these event files.

Even though the observations were carried out in 1/4 window mode, we nonetheless suffered from pileup at the source position. Hence, the spectra were extracted using an annular extraction region extending from 30 to 250 pixels from the source position. This extraction region size was chosen so as to extract >99% of the point source flux. As the outer radius of this annulus is larger than the window size (∼280, 295, 280 pixels, respectively), the effective extraction region is the intersection of window and the annulus. The resulting extraction region has an area equivalent to 62% of the 250 pixels outer radius; hence, we expect to have detected a commensurate percentage of the total source flux.

Background spectra were extracted from a source-free region of the detector; these are automatically scaled to match the data during the spectral analysis. Response files were generated using the tasks XISRMFGEN and XISSIMARFGEN. The background and response files were then grouped with the science spectrum for analysis in XSPEC.

[4] http://heasarc.nasa.gov/docs/suzaku/aehp_data_analysis.html

2.2. Hard X-ray Detector

The HXD covers the energy range from 10–600 keV, consisting of two separate detectors, (1) PIN: Silicon PIN photodiodes covering the energy range 10–70 keV and (2) GSO: GSO/BGO phoswich scintillators, covering the energy range 40–600 keV. Due to the arrangement of the instrument, with the PIN diodes residing in front of the GSO scintillator in each of the 16 detector units that make up the HXD, the raw data do not differentiate between the PIN and GSO, with this distinction instead being made during the extraction process.

As at the time of writing, the GSO analysis procedure had not been included in the official *Suzaku* data reduction pipeline, all of the hard X-ray detector data were reprocessed following the prescription in the abc guide and the 7-step guide.[5] GTI science events were extracted using XSELECT with the appropriate GTI files and filter options, i.e., pointing elevation $> 5^\circ$ above earth and excluding data taken near the SAA. The relevant events for each detector were then extracted by requiring DET_TYPE = 1:1 and DET_TYPE = 0:0 for the PIN and GSO, respectively.

The relevant background and response (pin/gso *20080129.rsp) files were obtained from the *Suzaku* Web site. A GTI between the data and the background file was then created using the ftool MGTIME, which was then used to extract the spectra in XSELECT. Standard corrections were applied to the data, i.e., dead time for science data, PIN background exposure time. As the HXD background files do not include the contribution from the cosmic X-ray background (CXB), the expected CXB was simulated following the recipe detailed in the abc guide; this was then added to the background file. As a check on the accuracy of the background, a separate background estimate was made using the earth occulted data (earth elevation = 0). This was found to be consistent with the above background.

A similar procedure is followed in the case of the GSO spectral extraction with the following caveat: the background file exposure time does not need to be corrected; instead one must rebin the science spectrum to match the provided background. The sensitivity of the GSO detector is background dominated; hence, the high-energy detection threshold is determined not by the statistical error but by the reproducibility of the background; here we conservatively estimate the background reproducibility to be 3% (e.g., Fukazawa et al. 2008). In Figure 2, we plot the extracted science and background spectra. *Swift* J1753.5−0127 is detected out to an energy of 250 keV

3. ANALYSIS & RESULTS

3.1. Light Curves

Source and background light curves were extracted from the event files using XSELECT and the appropriate good-time-interval events after the application of the appropriate baryocentric correction using the ftool AEBARYCEN. The flux from *Swift* J1753.5−0127 is observed to remain constant throughout our observation. The mean count rates for each individual detector are approximately: 16.2, 20.8, 17.1, 2.6, 2.2 counts s^{-1}(XIS0, XIS1, XIS3, PIN, GSO).

There is no evidence for any periodic modulation; the light curves across all detectors are characterized by rapid variability of a stochastic nature as is expected from accretion processes in the vicinity of a black hole (van der Klis 2006). This is consistent with *RXTE* power spectra bracketing these data that revealed a power-law slope, $\beta \sim -1$.

[5] http://www.astro.isas.ac.jp/suzaku/analysis/7step_HXD_20080114.txt

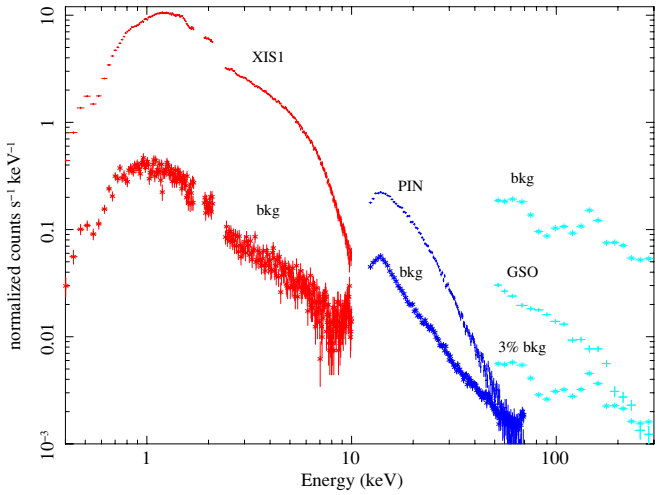

Figure 2. Background subtracted XIS1, PIN, and GSO spectra and their associated background spectra. For clarity, we plot only a single XIS detector. *Swift* J1753.5−0127 is detected by the PIN detector out to 60 keV, while the GSO detects flux to ∼250 keV assuming that the background is reproducible to an accuracy of 3% (see the text).

(A color version of this figure is available in the online journal.)

3.2. Spectra. I. Phenomenological Models

We initially choose to fit the spectra with a number of phenomenological models in an effort to provide a broad characterization of the data. Initial spectral fits were made to the entire data set consisting of five spectra in total (XIS0, XIS1, XIS3, PIN, GSO), spanning the energy range 0.6–250 keV over which *Swift* J1753.5−0127 is reliably detected. Explicitly, the spectra provide us with data in the following ranges: XIS0, XIS3 0.4–10 keV; XIS1 0.2–10 keV; PIN 12–70 keV, and GSO 50–250 keV. Unfortunately, the low-energy response of the XIS detectors contains a number of uncertain residuals; hence, we additionally ignored the regions below 0.6 keV and between 1.7–1.9 keV and 2.1–2.4 keV in all further modeling.

Initially, the column density was fixed at a value consistent with previous detections ($N_H = 2.3 \times 10^{21}$ cm^{-2}; Miller et al. 2006a), while the normalization was allowed to vary independently for each spectrum. The resulting normalizations were found to be consistent with those expected for the *Suzaku* detectors. The spectra were fit with a model consisting of an absorbed power law (`pha*po`),[6] which provided an acceptable fit except at the lowest energies ($\leqslant 2$ keV). As the main residual was present at energies below 2 keV, this region was ignored in further fitting. Re-applying the power-law fit results in a value for the spectral index of $\Gamma = 1.62$ ($\chi^2/\nu = 6968/6463$). It is immediately apparent that a simple phenomenological power-law model suffices to describe the spectrum from 2 to 250 keV.

The data were also fit with a `cutoffpl` model for comparison. The fit does not indicate the presence of a cutoff in the spectrum with the `cutoffpl` model fit being significantly inferior to a simple power law, i.e., we find $\chi^2/\nu_{po} = 6898/6463$ (6968/6456) and $\chi^2/\nu_{cutoffpl} = 6962/6462$ (7048/6455) for the $N_H = 0.18(0.23) \times 10^{21}$ cm^{-2} models, respectively. In both cases, the best-fit cutoff power-law model requires the high-energy cutoff to be 500 keV, i.e., the intrinsic upper limit of the

[6] Throughout this paper the abundances and cross-sections assumed are `bcmc` (Balucinska-Church & McCammon 1992) and `angr` (Anders & Grevesse 1989) respectively.

Table 1
Spectral Fit Parameters I

Model	Parameter	Value			
`phabs`	$N_{\rm H}[10^{22}\ {\rm cm}^{-2}]$	0.23		0.18	
	i	30	63.256	30	63.256
`po`	Γ	1.619 ± 0.003	1.619 ± 0.003	1.608 ± 0.003	1.608 ± 0.003
χ^2 ($\nu = 6456$)		6938	6938	6869	6869
`reflect*po`	Γ	1.640 ± 0.005	1.649 ± 0.006	1.625 ± 0.005	1.632 ± 0.005
	$f[\Omega/2\pi]$	0.17 ± 0.03	0.33 ± 0.05	0.14 ± 0.03	0.26 ± 0.05
χ^2 ($\nu = 6455$)		6830	6807	6793	6778
`reflect*po+laor`	Γ	1.645 ± 0.005	1.654 ± 0.005	1.630 ± 0.005	1.637 ± 0.005
	$f[\Omega/2\pi]$	$0.15^{+0.03}_{-0.02}$	0.27 ± 0.05	0.12 ± 0.03	0.21 ± 0.05
	$E_{\rm line}$[keV]	6.4 ± 0.1	6.4 ± 0.1	6.4 ± 0.1	6.4 ± 0.1
	$R_{\rm in}[R_g]$	13^{+7}_{-4}	19^{+4}_{-5}	13^{+7}_{-5}	19^{+6}_{-4}
	EW[eV]	60 ± 30	80^{+50}_{-40}	60^{+20}_{-35}	70 ± 30
χ^2 ($\nu = 6451$)		6743	6720	6707	6694
`reflect*(diskbb+po)+laor`	$T_{\rm diskbb}$[keV]	0.190 ± 0.002	0.180 ± 0.003	0.25 ± 0.03	0.20 ± 0.04
	$\rm norm0_{diskbb}$	3866 ± 420	4830^{+620}_{-470}	137^{+124}_{-63}	361^{+1052}_{-232}
	$\rm norm1_{diskbb}$	4023 ± 410	5080^{+600}_{-460}	115^{+97}_{51}	294^{+780}_{-183}
	$\rm norm3_{diskbb}$	4144 ± 460	5340^{+670}_{-530}	135^{+136}_{-66} 76	432^{+1536}_{-293}
χ^2 ($\nu = 7442$)		8349	8282	8160	8149

Notes. Results of fits to the *Suzaku* spectra for *Swift* J1753.5−0127, spanning the energy range 0.6–150 keV. All models are modified by "`pha`" to account for interstellar extinction, which was frozen at the value indicated in the table above. In addition, the spectral regions below 0.6 keV and between 1.7–1.9 keV and 2.1–2.4 keV are ignored at all times due to the presence of instrumental calibration uncertainties. All errors are quoted at the 90% confidence level.

`cutoffpl` model. Ignoring the data above 150 keV does not improve the quality of the `cutoffpl` fit relative to the `po` fit.

As the GSO background contains a large feature in the energy range 150–180 keV (see Figure 2), we decided to ignore the data beyond 150 keV in all further fitting. Furthermore, as there is clearly an additional component contributing at energies below 2 keV, this region is ignored while constraints are placed on the hard X-ray emission. Repeating the above power-law fit, we find $\Gamma = 1.61$ ($\chi^2/\nu = 6869/6456$).[7]

Inspection of the residuals reveals any contribution from disk reflection to be small, although there is evidence for curvature in the PIN spectrum. To investigate the possible contribution due to disk reflection, the best-fit power law from above was convolved with the reflection model of Magdziarz & Zdziarski (1995; `reflect*po`). The inclination was held fixed ($\cos i = 0.45$), while the abundances of metals were frozen at the default values ($N_Z/N_\odot = 1$). The best-fit model reveals a slightly softer power law ($\Gamma \sim 1.63$) in addition to a highly significant ($>9\sigma$ as determined via an F-test) reflection fraction, $f \sim 0.26$ ($\chi^2/\nu = 6778/6455$). As the measured spectral parameters depend on the inclination angle, these and subsequent fits were repeated at a lower inclination angle of 30°. These fits revealed a lower reflection fraction, $f \sim 0.14$ (see Table 1).

Closer inspection of the XIS spectra residuals reveals a slight excess consistent with the presence of a broad Fe K line. To place a constraint on the size of any possible line, a Gaussian was added to this model. The best energy of this line is $\sim$6.4 ± 0.1 keV, in agreement with that expected from neutral Fe Kα. This is consistent with that expected from reflection from neutral matter ($E_{\rm line} = 6.4$ keV) as assumed in the `reflect` model. The Gaussian component was then replaced with relativistic line model (`laor`; Laor 1991), which more accurately represents the expected line profile in the inner disk region. The inclination of this line is fixed at the same value as the reflection component, the emissivity profile of the disk is fixed at R^{-3}, and the outer radius of the emitting region is fixed at 400 R_g. We find that the data require the presence of a broad weak iron line ($>8\sigma$ significant as determined via an F-test; EW = 73 ± 30 eV). Allowing the inner disk radius to vary, we find $R_{\rm in} = 19^{+6}_{-4} R_g$. The iron line inner radius has a strong inclination dependence with a best fit $R_{\rm in} \sim 13 R_g$ at 30°. The above inner radii are inconsistent with the ISCO for a Schwarzschild black hole; if we extend the confidence intervals, we place the following limits on the inner radius: $R_{\rm in} \geqslant 11 R_g$ and $6.8 R_g$ (3σ level) for inclinations of 63.°256 and 30° ($\cos i = 0.45$, 0.8660), respectively.

Including the lower energy flux in the fit once again, results in a chi-squared value of $\chi^2/\nu = 9431/7450$, we plot this in Figure 3. A soft excess is present consistent with previous observations, i.e., Miller et al. (2006a). A simple blackbody accretion disk component (`diskbb`; Mitsuda et al. 1984) was added to this model to account for the excess soft X-ray flux, while the power-law index, Γ, and the reflection fraction, f, were frozen at their previous best-fit values. The disk component is strongly required by the data; the best fit is achieved for a disk temperature of kT = 0.20 keV ($\chi^2/\nu = 8149/7442$). We measure the associated 0.6–10 keV (2–150 keV) unabsorbed flux to be 6.8×10^{-10} erg s^{-1} cm^{-2} (2.4×10^{-9} erg s^{-1} cm^{-2}).

The column density is crucial here, although it has little impact on the spectrum above energies $\sim$2 keV, it will have a significant impact on the shape of the spectrum and the measured flux below this value, e.g., Figure 3. In order to test the effect of different values for $N_{\rm H}$, the fitting was repeated at a number of different values for the interstellar column density ranging from $N_{\rm H} = 0.17 \times 10^{22}$ cm^{-2} (Dickey & Lockman 1990) to 0.28×10^{22} cm^{-2} (Schlegel et al. 1998). We find the best fit as measured by *Suzaku* to be $\rm N_H = (0.18 \pm 0.01) \times 10^{22}$ cm^{-2}. In

[7] All further fits in this section assume $N_{\rm H} = 0.18 \times 10^{21}$ cm^{-2} unless otherwise explicitly stated

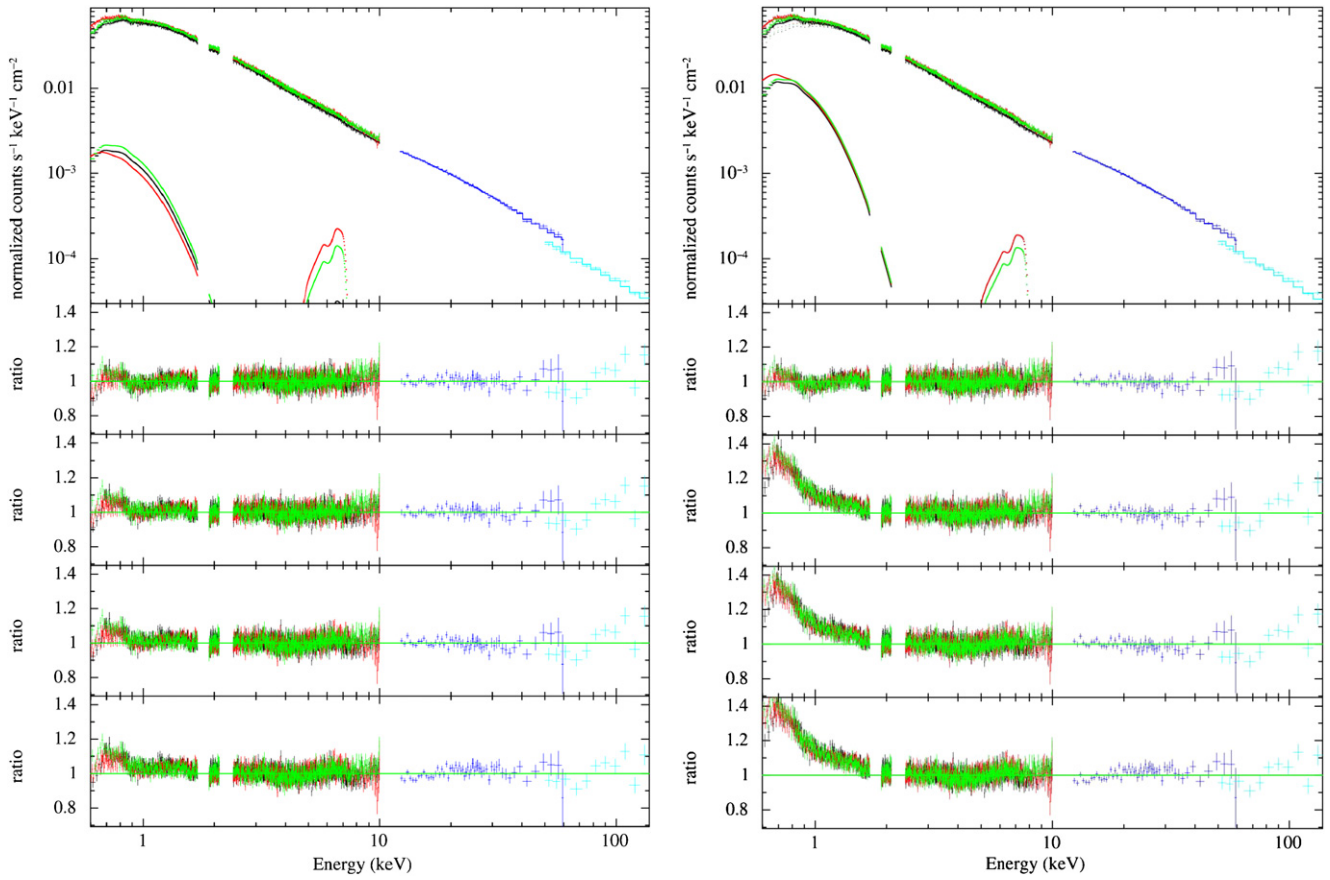

(a) $N_H = 0.18 \times 10^{22}$ cm^{-2}, i $\sim$ 63 (b) $N_H = 0.23 \times 10^{22}$ cm^{-2}, i $\sim$ 63

Figure 3. Best fit to the *Suzaku* spectra of *Swift* J1753.5−0127 in the 0.6–150 keV range. The best-fit model consisting of a disk blackbody plus power law modified by disk reflection (`pha*(reflect*(diskbb+po)+laor)`) is plotted. The residuals show from bottom to top `pha*po`, `pha*(reflect*po)`, `pha*(reflect*(po)+laor)`, and `pha*(reflect*(diskbb+po)+laor)`. There is a clear excess at soft X-ray energies, the solid lines denote the `diskbb` & `laor` components. The regions 1.7–1.9 keV and 2.1–2.4 keV are ignored due to the presence of instrumental features.

(A color version of this figure is available in the online journal.)

Table 1, we list the parameters for the best-fit model and also those for the model corresponding to the value of N_H measured previously by *XMM-Newton*.

The normalization of the `diskbb` model is proportional to the inner disk radius, norm $= (r_{in}$ [km])/d [10 kpc])$^2 \cos\theta$. In Figure 4, we plot the inner disk radius corresponding to the best-fit `diskbb` component for various values of the column density, where we have corrected for spectral hardening and the inner disk radius (see Section 4.2). We find that for reasonable values of the column density and inclination the inner disk radius may reside close to the ISCO, in agreement with recent work, which has provided evidence that the cool disk may reside at or near the ISCO, even at the low luminosities typically observed in the LHS (Miller et al. 2006a, 2006b; Tomsick et al. 2008). We also modeled the soft excess using the `ezdiskbb` and `diskpn` models in XSPEC. In both cases, the observed blackbody component is found to be consistent with that obtained using `diskbb`. We also experimented with using the `kdblur` kernel to relativistically blur the above continuum model; however, this did not result in an improved fit.

We also carried out fits to the individual telemetry segments of the XIS, PIN, and GSO spectra to check for possible variability. The fits to each of the three segments were found to be consistent with each other; hence, there is no evidence for spectral variability in agreement with the constant flux observed from the light curves.

3.3. Spectra. II. Physically Motivated Models

While the above models provide an excellent fit to the observed data, due to their phenomenological nature they offer limited constraints on the nature of the accretion flow. In this section, we will consider more complex models in an effort to place improved constraints on the physical processes that create the observed spectrum. We consider two scenarios for the observed spectrum: (1) the observed spectrum is the result of the reflection of hard X-rays from a power law incident on the accretion disk, and (2) the spectrum is due to emission from a Comptonizing corona.

1. *Disk reflection models*. Observations of a number of AGN and Galactic black holes have revealed disk reflection features, the most prominent of which are the Fe K line at ∼6.4 keV and the reflection bump at ∼20–30 keV. The constant density ionized disk model (`CDID`; Ross & Fabian 1993; Ballantyne et al. 2001) is used to model this effect. Here, we only consider data below 60 keV as the `CDID` model as implemented in XSPEC is not valid at energies above 100 keV. Solar metallicity is assumed in these fits. As a check, a power-law fit to the 2–60 keV region of the spectrum alone was carried out; the resulting power-law index is found to be in agreement with the value derived from a fit to the entire spectrum (Section 3.2). Initially, the spectrum was fit with the `CDID` model alone modified by

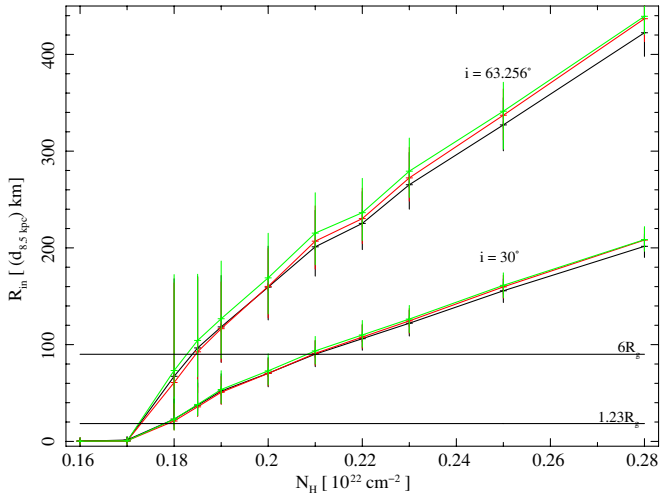

Figure 4. Inner disk radius for the cool multi-color blackbody accretion disk `diskbb` component vs. column density, where we have corrected for spectral hardening and the inclination (see the text). The two sets of lines indicate the expected inner radius assuming an inclination of 30° and 63°256, respectively. The error bars correspond to the 90% confidence interval for the disk normalization. The horizontal lines indicate the position of the ISCO for both a Kerr ($1.23R_g$) and Schwarzschild ($6R_g$) black hole, where the black hole mass is assumed to be 10 $M_\odot$ ($R_g \equiv GM/c^2$).

(A color version of this figure is available in the online journal.)

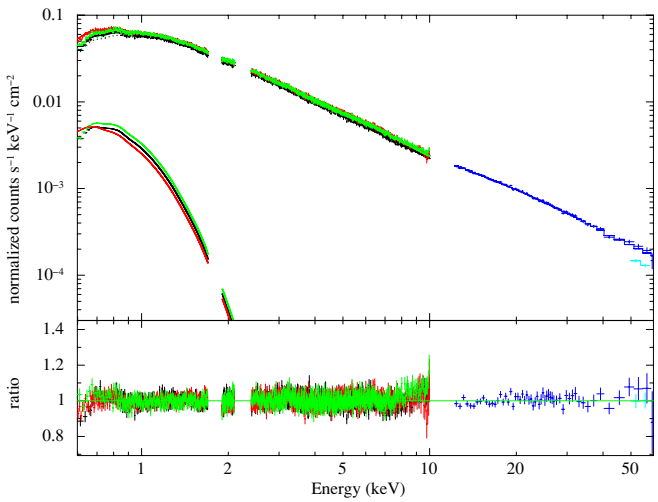

Figure 5. Best-fit disk reflection model (`pha*(diskbb+CDID)`) to the *Swift* J1753.5−0127 spectrum; see Section 3.3 for details. The inferred inner disk radius is low and consistent with that measured in Section 3.2. See Table 2 for the model parameters.

(A color version of this figure is available in the online journal.)

interstellar absorption; the resulting fit was good ($\chi^2/\nu = 8070/7428$), with a moderately ionized disk ($\xi \sim 3.55$) and a reflection fraction ($f \sim 0.14$) in agreement with that measured earlier. A blackbody accretion disk component was added to this model significantly improving the fit ($\chi^2/\nu = 8017/7424$, $> 6\sigma$ significant as measured by an F-test). For our best-fit model `pha*(diskbb+CDID)`, we find the following parameters $N_H \sim 0.20$, $T_{ddiskbb} \sim 0.19$, $\xi \sim 3.55, \Gamma \sim 1.61$, and $f \sim 0.12$; see Table 2 and Figure 5. The disk is found to be moderately ionized, while the low-reflection fraction is consistent with the absence of any large reflection features in the observed spectrum. The disk temperature in this model is consistent with that found assuming a simple `diskbb+po` model (see Section 3.2), $T_{diskbb} \sim 0.19$ keV. The inner radius in this case is $\sim 70 \cos\theta^{-1} d_{8.5\ \mathrm{kpc}}$km. We note that for inclinations less than 39° this is less than the radius of the ISCO for a 10 $M_\odot$ Schwarzschild black hole.

2. *Comptonizing corona models*. X-ray spectra of black hole binaries in the LHS are typically modeled assuming that the hard X-ray flux originates in a corona lying above the accretion disk, which then scatters the soft X-ray flux from the disk to higher energies. *Suzaku* observations of GRO J1655−40 and Cyg X-1 have been modeled in such a manner (Takahashi et al. 2008; Makishima et al. 2008); here, we model the broadband spectrum of *Swift* J1753.5−0127 following the Comptonization model outlined in the above papers.

Initial fits with a single Comptonizing component were found to provide an inadequate fit, particularly at the highest energies. As in the cases of GRO J1655−40 and Cyg X-1 above, we model the spectrum using a pair of Comptonizing coronae with the same electron temperature but differing optical depths (`diskbb+compps+compps+laor`), where a `laor` component is added to account for the possible presence of a relativistic iron line. A spherical geometry was assumed for the Comptonizing cloud, and possible disk reflection effects were accounted for using the reflection routine built into the `compps` model. First, the fit was carried out without the accretion disk component (i.e., `pha(compps+compps)`) to check if this component was actually required, the best fit is good ($\chi^2/\nu = 8173/7430$). However, the column density is large ($N_H \sim 0.28 \times 10^{22}$ cm^{-2}), while the seed temperature is low ($T_{in1} = T_{in2} = 0.1$ keV). Significant disk reflection is not required in this model.

Addition of an accretion disk to this model significantly improved the quality of the fit, with a reduced chi-squared of 1.09 ($\chi^2/\nu = 8086/7427$). The disk component is not required in the fit to the XIS0 spectrum; however, the 90% upper limit to the disk normalization is consistent with the value measured from the XIS1 & XIS3 spectra. Again we note that the value returned for the interstellar extinction $N_H \sim 0.31 \times 10^{22}$ cm^{-2} is much higher than any previously measured value, and as such would appear to be inconsistent with expectations for N_H in the direction of *Swift* J1753.5−0127 (see Section 4.1). The iron line component also significantly improved the fit ($\chi^2/\nu = 8009/7422$; see Figure 6), where the inner radius is $\sim 60\ R_g$.

In the best-fit model above the temperature of the electrons in the corona is low $kT_e \sim 53$ keV, while the optical depths are found to be approximately 0.34 and 2.57 for the two Comptonizing components, respectively; see Table 2. We may estimate the size of the optically thin ($\tau \sim 0.34$) and optically thick ($\tau \sim 2.57$) regions of the Comptonizing cloud from the normalization, where the radius of the spherical cloud is $R \sim d_{10\ \mathrm{kpc}} \times (\cos\theta \times \mathrm{norm})^{0.5}$. In both cases, the inferred radius is small $\sim 305 \cos\theta^{0.5}$ km and $540 \cos\theta^{0.5}$ km ($\sim 20 R_g$ and $36 R_g$ assuming a 10 $M_\odot$ black hole and a distance of 8.5 kpc) for the optically thick and optically thin regions, respectively. The temperature of the seed disk component is low at 0.1 keV. We note that this is approximately half the value for the blackbody temperature one finds when fitting the data assuming a simple reflection continuum (see Section 3.2) or when fitting the data with a detailed reflection model (see Section 3.3, item 1). As the temperature is low and the lower limit to our data is only 0.6 keV, the disk normalization is poorly constrained as may

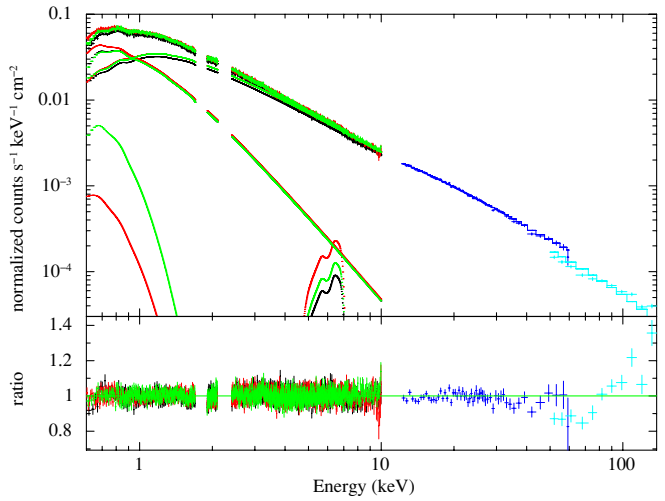

Figure 6. Best-fit Comptonization model (`pha*(diskbb+compps+compps+laor)`) to the *Swift* J1753.5−0127 spectrum; see Section 3.3 for details. The inferred inner disk radius is larger than that measured in Section 3.2, i.e., $R_{\rm in} \gtrsim 30R_g$. See Table 2 for the model parameters.

(A color version of this figure is available in the online journal.)

be seen by inspection of Table 2. Nonetheless, the inner radius of the accretion disk is consistent with overlapping with the coronal region (i.e., $R_{\rm in-disk} \approx R_{\rm corona}$ within the errors).

4. DISCUSSION

We present *Suzaku* broadband spectra (0.6–250 keV) of the black hole candidate *Swift* J1753.5−0127 while in the LHS. The observed spectrum is measured to be consistent with an unbroken power law, $\Gamma \sim 1.63$. During our observation, the flux from the source was observed to be constant, with a 0.6–150 keV unabsorbed flux of 2.6×10^{-9} erg s^{-1} cm^{-2} ($L_x/L_{\rm Edd} = 0.016 d^2_{8.5\ {\rm kpc}} M_{10M_\odot}$). This is consistent with *INTEGRAL* observations of GRO J1655−40 in the LHS where unbroken power-law emission ($\Gamma \sim 1.72$) extending out to $\sim$500 keV was detected at a luminosity of $\sim 0.015\ L_{\rm Edd}$ (Caballero Garcia et al. 2007; although see Joinet et al. 2008).

4.1. Column Density : $N_{\rm H}$

Accurate determination of the interstellar column density is crucial due to the preferential absorption of soft X-rays, which in our case are consistent with being emitted by the cool accretion disk. Measurement of $N_{\rm H}$ is best achieved at soft X-ray energies. Here, *XMM-Newton* with its well-studied low-energy calibration should provide the most reliable determination of the interstellar column density $N_{\rm H} = 0.23 \times 10^{22}$ cm^{-2} (Miller et al. 2006a). In contrast, the best-fit value as measured with *Suzaku* is $N_{\rm H} = 0.18 \times 10^{22}$ cm^{-2}. However, we do note that the measured $N_{\rm H}$ depends on the continuum model assumed, e.g., for the Comptonizing corona model we find a best-fit value $N_{\rm H} = (0.31 \pm 0.01) \times 10^{22}$ cm^{-2}.

In order to investigate the instrumental dependence of our measured values of the column density, we also fit the best-fit models above to a number of *Swift* XRT spectra taken before and after our *Suzaku* observation, with the closest occurring $\sim$60 days beforehand (obsid: 00030090050). The results from these fits are consistent with the results of our fits to the *Suzaku* spectrum, with the caveat that the smaller energy coverage (0.6–10 keV versus 0.6–150 keV) and exposure time ($\sim$2 ks) necessarily result in larger confidence regions from fits to the *Swift* spectra.

Table 2
Spectral Fit Parameters II

Model	Parameter	Value
`phabs`	$N_{\rm H}[10^{22}\ {\rm cm}^{-2}]$	0.20 ± 0.01
`diskbb+cdid`	$T_{\rm diskbb}$[keV]	0.19 ± 0.01
	${\rm norm}_{\rm xis0}$	1554^{+824}_{-783}
	${\rm norm}_{\rm xis1}$	1554^{+1222}_{-670}
	${\rm norm}_{\rm xis3}$	1554^{+1338}_{-886}
	Γ	1.614 ± 0.002
	$f[\Omega/2\pi]$	$0.12^{+0.02}_{-0.01}$
	ξ[erg s^{-1} cm^{-2}]	$3.47^{+0.08}_{-0.05}$
	χ^2 ($\nu = 7424$)	8017
	Parameter	Value
`phabs`	$N_{\rm H}[10^{22}\ {\rm cm}^{-2}]$	0.31 ± 0.01
`diskbb+compps`	$T_{\rm diskbb}$[keV]	0.10 ± 0.01
`+compps+laor`	${\rm Norm}_{\rm xis0}$	$\leqslant 3.3 \times 10^5$
	${\rm Norm}_{\rm xis1}$	$(0.35^{+1.7}_{-0.2}) \times 10^5$
	${\rm Norm}_{\rm xis3}$	$(1.84 \pm 1.4) \times 10^5$
	KT_e[keV]	53 ± 3
	T_{in1}[keV]	$T_{\rm diskbb}$
	τ_1	0.34 ± 0.01
	${\rm Norm}_{\rm compps1}$	$(4.14^{+0.13}_{-0.21}) \times 10^5$
	$T_{\rm in2}$[keV]	$T_{\rm diskbb}$
	τ_2	$2.57^{+0.01}_{-0.05}$
	${\rm Norm}_{\rm compps2}$	$(1.28^{+0.05}_{-0.02}) \times 10^5$
	$f[\Omega/2\pi]$	$\leqslant 0.01$
	$E_{\rm line}$[keV]	6.4 ± 0.1
	$R_{\rm in}[R_g]$	60^{+70}_{-25}
	EW[eV]	70 ± 30
	χ^2 ($\nu = 7422$)	8009

Notes. Parameters for the physically motivated models from Section 3.3. All errors have been calculated using the `error` command in XSPEC and are quoted at the 90% confidence level. For `compps` models the inclination is frozen at 63.°256 due to the spherical geometry of the corona the inclination dependence of this model is negligible.

These measurements are in agreement with numerous independent measures of the interstellar column, sourced both from direct measurements and Galactic surveys. X-ray observations from *Swift* measured a column density of 0.20×10^{22} cm^{-2} (Morris et al. 2005), while optical measurements also require $N_{\rm H} = 0.2 \times 10^{22}$ cm^{-2} (Cadolle Bel et al. 2007). Additionally, an estimate of the column density may be obtained from various radio ($N_{\rm H} = 0.17 \times 10^{22}$ cm^{-2}, Dickey & Lockman 1990; 0.17×10^{22} cm^{-2}, Kalberla et al. 2005) and far-IR (0.28×10^{22} cm^{-2}, Schlegel et al. 1998) surveys.

The radius of the cool disk component depends on the column density and inclination as illustrated in Figure 4. From above, we see that for the directly measured values of $N_{\rm H}$ toward *Swift* J1753.5−0127, the observed soft excess may originate from an accretion disk whose inner radius is consistent with the ISCO.

4.2. A Thin-disk at the ISCO

The significant soft excess observed in *Swift* J1753.5−0127 (Figure 3) is consistent with an origin in a standard multi-color blackbody accretion disk (Mitsuda et al. 1984 and see Table 1). The disk normalization may be used to estimate the inner radius of the accretion disk when knowledge of the distance and inclination are available, as norm $\sim (r_{\rm in}/d_{10\ {\rm kpc}})^2 \cos\theta$. This estimate is subject to a number of corrections: (1) spectral

hardening must be accounted for, typically this requires a multiplicative correction factor ~ 1.7 (Shimura & Takahara 1995) and (2) one must correct for the inner radius, where $R_{\rm in} = 1.18 r_{\rm in}/\sqrt{\cos\theta}$ (Makishima et al. 2000). There are also additional errors, i.e., the zero torque inner boundary condition (Zimmerman et al. 2005) and radiative transfer effects (Merloni et al. 2000), which could contribute but are difficult to quantify.

In Figure 4, we plot the inner disk radius (corrected for (1) and (2) above) measured from our best-fit models in Section 3.2. The best-fit radius is consistent with the ISCO, for certain values of $N_{\rm H}$ and inclination, although there are large uncertainties. Previous observations of *Swift* J1753.5−0127 at a 0.5–10 keV flux of 3.9×10^{-10} erg s^{-1} cm^{-2} detected a cool accretion disk with an inner radius consistent with the ISCO. The measurements presented herein, at an unabsorbed 0.6–10 keV flux of 6.8×10^{-10} erg s^{-1} cm^{-2}, are in agreement with the previous analysis of Miller et al. (2006a) and furthermore a test to the stability of the cool disk component given that the observations were separated by almost 18 months (see Figure 1).

Miller et al. (2006b) observed GX 339−4 at a luminosity of $\sim$0.05 $L_{\rm Edd}$ with *XMM-Newton* and *RXTE*. A significant excess of soft X-ray flux was detected in the *XMM-Newton* data alone, due to the absence of soft X-ray coverage for *RXTE*. Modeling revealed this excess to be consistent with a cool accretion disk ($kT_{\rm in} \sim 0.35$ keV) extending to the ISCO. Subsequent observations utilizing both *RXTE* and *Swift* at luminosities of 0.023 and 0.008 $L_{\rm Edd}$ also detected this excess soft X-ray component (Tomsick et al. 2008). Together with the new observations presented in this paper, these results appear to confirm the presence of the inner radius of the accretion disk at the ISCO (or at least at a radius far lower than expected) for luminosities far below that at which the state transition from HSS to LHS state occurs in contrast to theoretical expectations (e.g., Esin et al. 1997).

Wilkinson & Uttley (2009) have re-analyzed the *XMM-Newton* data on *Swift* J1753.5−0127 and GX 339−4 focusing on the timing characteristics and variability inherent to the spectra. Using a new analysis technique, they find significant evidence for the presence of the soft spectral component in agreement with Miller et al. (2006a, 2006b). They interpret the soft X-ray flux as originating in variability intrinsic to the accretion disk. In particular, they find that the intrinsic variability of the accretion disk is likely to be responsible for the low-frequency Lorentzian feature present in the power spectral density function of sources in the LHS. This places a limit on the disk truncation radius of $< 20\ R_g$. The *XMM-Newton* spectrum of *Swift* J1753.5−0127 has also been re-analyzed by Reis et al. (2009). They fit the spectrum with a relativistically blurred reflection model and find an inner disk radius of $R_{\rm in} \sim 3R_g$. This in turn provides a measure of the spin of the putative black hole of $a \sim 0.76$. Again, inconsistent with the idea of a large truncation radius for the accretion disk in the LHS.

The magnitude of the reflection features is observed to be quite low in our data. Although the presence of a broad relativistic line is required by the data ($>7\sigma$ significant, EW $\sim 70 \pm 30$ eV), it is intrinsically weak (norm $\sim 10^{-4}$). The detection of a relativistic iron line is consistent with the measurements of Durant et al. (2009) who also measured a redshifted line at an energy of 6.2 keV during pointed *RXTE* observations (see Figure 1). The inner radius inferred from the `laor` line fits is larger than the ISCO at $R_{\rm in} \sim$ 10–20 gravitational radii, although much less than might be expected from the standard disk picture for disk truncation, where the inner radius is expected to be an order of magnitudes larger (Esin et al. 1997).

The curvature present in the PIN spectrum is also consistent with a low reflection fraction, $f \sim 0.12$–0.21 (inclination $\sim 30^\circ$–$63^\circ.256$). We note that the reflection fraction inferred from the self-consistent `CDID` model is at the lower end of the values inferred from the phenomenological `reflect*(diskbb+po)+laor` model. It is known that the reflection features of black hole binaries are generally weaker in the LHS than in higher luminosity states (i.e., Miller et al. 2002, 2004). The relative weakness of these features in *Swift* J1753.5−0127 is primarily due to the low luminosity nature of the source ($L_x \sim 8 \times 10^{36}$ erg s^{-1}). In comparison, the X-ray luminosity in GX 339−4 (Miller et al. 2006b) was much higher when a strong relativistically smeared iron line ($\sim 8\sigma$ significant, EW ~ 350 eV) was detected ($L_x \sim 4 \times 10^{37}$ erg s^{-1}).

The value we measure for the reflection fraction in *Swift* J1753.5−0127 is comparable to previous LHS observations where reflection fractions of $\sim$0.2–0.3 were measured in Cyg X-1 and GX 339−4 (Gierlinski et al. 1997; Miller et al. 2006b). In contrast, observations at higher luminosities require much higher reflection fractions. X-ray spectra of the black hole binaries XTE J1650−500 and GX 339−4 in the VHS state revealed reflection fractions of approximately unity (Miller et al. 2002, 2004). The low reflection fractions inferred in the LHS may be interpreted as evidence for a truncated disk, e.g., Gierlinski et al. (1997). Alternatively, the disk may remain close to the ISCO with the low reflection fraction resulting from beaming of the hard X-ray flux away from the disk by a mildly relativistic outflowing corona, e.g., Beloborodov (1999).

4.3. Alternatives to a Thin Disk at the ISCO

A number of alternative explanations have been put forward to account for the presence of the soft excess observed in *Swift* J1753.5−0127 and GX 339−4. Hiemstra et al. (2009) re-analyzed the data from Miller et al. (2006a) and find that while it is consistent with containing a soft disk component, a number of alternative continuum prescriptions that allow the disk to be truncated are also valid; however, see Reis et al. (2009) and Wilkinson & Uttley (2009) who outline a number of issues with this result.

Gierlinski et al. (2008) propose a scenario in which the disk is truncated at larger radii; however, the inner edge of the disk is irradiated by the high-energy Comptonized photons in the corona. This irradiation will cause the truncated inner disk edge to be hotter and hence appear to lie at smaller radii than is actually the case. In the model of D'Angelo et al. (2008), the inner edge of the cool truncated disk is seen to overlap with the inner ADAF region. Here, in the overlap region, the cool disk is heated to temperatures mimicking those of a cool disk at the ISCO.

It is also possible that what we observe is not the accretion disk but instead a ring of material that has condensed from the corona. Such an idea has been explored in detail by Liu et al. (2007) and Taam et al. (2008). They find that it is possible for enough material to condense from the corona to produce an inner ring of material extending from near the ISCO to a few tens of Schwarzschild radii, while the accretion disk is truncated at larger radii. In particular, detailed modeling was able to reproduce the soft disk components observed by Tomsick et al. (2008) in GX 339−4 (see Taam et al. 2008).

Table 3
Comptonizing Corona Fits to the Spectra of Low-hard State Black Holes Observed by *Suzaku*

System	L_x ($L_{\rm Edd}$)	N_H (10^{21} cm^{-2})	kT_{bb} (keV)	R_{disk} (km)	R_{thick} (km)	R_{thin} (km)	kT_e (keV)	τ_1	τ_2	f ($\Omega/2\pi$)
Swift J1753.5−0127	0.016	0.31	0.1	∼830	∼205	∼360	53	0.34	2.57	0
GRO J1655−40	0.007	0.74	0.2	∼330	∼26	∼65	135	0.25	1.2	0.5
Cyg X-1	0.02	0.66	0.3	∼103	∼75	∼200	100	0.4	1.5	0.4

Notes. GRO J1655−40 data from Takahashi et al. (2008), Cyg X-1 data from Makishima et al. (2008), *Swift* J1753.5−0127 data from this work. Where required, a distance of 8.5 kpc and an inclination of 63°.256 have been assumed for *Swift* J1753.5−0127. R_{disk} refers to the inner radius of the accretion disk, whereas R_{thick} and R_{thin} refer to the outer radius of the optically thick and thin regions of the Comptonizing cloud, respectively.

4.4. Comparison with Previous Suzaku Observations

Two additional black hole binaries have been observed by *Suzaku* while in the LHS. Takahashi et al. (2008) presented observations of GRO J1655−40, while Makishima et al. (2008) observed Cyg X-1. The observations took place while the systems were in the LHS at luminosities of approximately 0.007 $L_{\rm Edd}$ and 0.02 $L_{\rm Edd}$, respectively. We also modeled the spectra of *Swift* J1753.5−0127 with a combination of two Comptonizing components, to aid comparison of these data to the *Suzaku* observations of the black hole binaries Cyg X-1 (Makishima et al. 2008) and GRO J1655−40 (Takahashi et al. 2008). For both of these systems, the observed spectrum was interpreted as being due to a two-component Comptonizing corona, i.e., a population of electrons with the same temperature (kT_e) but differing optical depths (τ), modified by disk reflection, `diskbb+compps+compps`. The parameters of our best-fit model are listed in Table 2, while the fit itself is displayed in Figure 6. In Table 3, we display the parameters for our best-fit Comptonization model along with those for the best-fit models for Cyg X-1 and GRO J1655−40.

The blackbody disk component is found to be cool ($kT \sim 0.1$ keV), and the inner radius of the accretion disk is consistent with the outer radius of the corona within the errors ($R_{\rm in} \sim 30R_g$). The best-fit radius for the iron line is also consistent with this value. The high value for the Hydrogen column density (0.31×10^{22} cm^{-2}) returned by this model is inconsistent with the available data and casts doubt on the Comptonization scenario as a viable model for the observed *Suzaku* spectrum of *Swift* J1753.5−0127. However, the presence of circumstellar matter or a local absorber could account for the excess absorption above that detected at radio wavelengths.

We find an electron temperature cooler than that measured in both Cyg X-1 and GRO J1655−40 when the spectra are interpreted in terms of this Comptonizing corona model. Assuming the disk truncation model for the LHS to be correct, we would expect the electron temperature to decrease with increasing luminosity, e.g., Esin et al. (1998). The value of kT_e we measure would imply that *Swift* J1753.5−0127 was at a luminosity in excess of that at which Cyg X-1 was observed (∼0.02 $L_{\rm Edd}$). This is in contrast to various luminosity estimates. Indeed, we measure a luminosity of $\sim 0.016 d^2_{8.5\ {\rm kpc}} M_{10\ M_\odot} L_{\rm Edd}$; for *Swift* J1753.5−0127 to have a luminosity greater than that of Cyg X-1 at the time of the *Suzaku* observations would imply a distance greater than 8.5 kpc and or a black hole mass less than 10 $M_\odot$.

Makishima et al. (2008) have argued that the inner radius of the accretion disk does not extend to the ISCO in the LHS state based on the *Suzaku* observations of Cyg X-1 and GRO J1655−40 (see Section 4.3). They base their argument around two main points; first, the low reflection fractions measured in the LHS state show that either the accretion disk does not intrude too deeply into the corona or some form of outflow must be formed. They consider the outflow case to be unlikely as the reflection fractions measured in both GRO J1655−40 ($i \sim 70°$) and Cyg X-1 ($i \sim 45°$) are similar, whereas if the reflection was due to an outflow it would be expected to have a strong inclination dependence, which is not observed. Here, we note that the errors on the reflection fractions measured in the case of Cyg X-1 ($f = 0.4^{+0.2}_{-0.3}$) call into question the validity of this inclination-based argument, given the quality of the currently available data.

Second, it is argued that the inner radius determined from fits to the iron K line in Cyg X-1 (∼$13R_g$) is inconsistent with the ISCO. This point is much more ambiguous as their reported value of the inner radius is $R_{\rm in} = 13^{+6}_{-7} R_g$. This value is consistent with the ISCO for a Schwarzschild black hole. As such, it is clear from the currently available data that there is evidence for a cool disk component, with an inner radius that in some cases is consistent with the ISCO, whether or not the cool disk component actually extends to the ISCO is presently not clear.

Finally, it is important to note the high-mass X-ray binary nature of Cyg X-1. Here the accretion process, namely accretion via a stellar wind, is significantly different from that in GRO J1655−40 (Roche lobe overflow) and as such may preclude detailed comparison with the low-mass X-ray binaries like *Swift* J1753.5−0127 and GRO J1655−40.

4.5. Jet and/or Corona

Our knowledge of role of the relativistic radio jets in X-ray binaries has advanced rapidly in the past 10 years. Observations of numerous X-ray binaries have revealed the presence of a compact quasi-steady jet in the LHS, whereas in the high-soft state the jet is typically observed to disappear (Fender et al. 2004, 2009). These also point toward a significant contribution from the jet toward the overall energy budget of the binary system, with the jet luminosity being possibly equal to that observed in X-rays, e.g., Gallo et al. (2005). In addition, a significant correlation has been found between the X-ray and radio luminosities of accreting sources across a range of luminosity (in Eddington units), suggestive of a disk–jet coupling (Gallo et al. 2003).

Markoff & Nowak (2004) have shown how one could, in principle, distinguish between different jet models based on the magnitude of the reflection features present in the spectrum. In particular, reflection fractions greater than 0.2 could not be reproduced by their jet models, reflection fractions between 0.1–0.2 could be due to synchrotron self-Comptonization in the base of a jet, while a reflection fraction below 10% could be interpreted as evidence that the spectrum was dominated

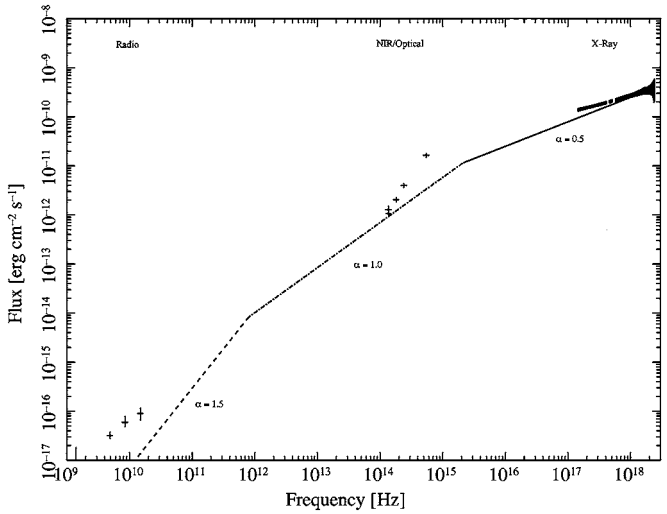

Figure 7. Absorption corrected spectral energy distribution for *Swift* J1753.5−0127. We assumed a column density of $N_{\rm H} \sim 0.20 \times 10^{22}$ cm^{-2} to facilitate comparison with the SEDs displayed in Cadolle Bel et al. (2007) and Durant et al. (2009). The optical/NIR and X-ray data are quasi-simultaneous; see Section 4.5 for details.

by synchrotron emission from the jet. If the base of the jet is confined within a few gravitational radii of the black hole, relativistic light bending will become important. This will act in the opposite direction to the beaming of the outflow leading to a slightly larger reflection fraction (Miniutti & Fabian 2004). These models are also consistent with the detection of an accretion disk near the ISCO, as we have likely detected with *Suzaku*.

A break or cutoff in the high-energy spectrum of black holes and neutron stars can be interpreted in terms of the electron temperature in a thermal Comptonizing corona. The high-energy spectrum of *Swift* J1753.5−0127 extends to at least 200 keV without a strong break or cutoff in our observations. Moreover, single thermal Comptonization models fail to achieve acceptable fits. In the context of Markoff & Nowak (2004), the reflection fraction of ∼0.12–0.21 measured in *Swift* J1753.5−0127 is consistent with a disk that is illuminated by synchrotron self-Comptonization produced in the base of a jet. A corona that is independent of a jet but which produces a non-thermal Comptonization spectrum might be able to describe the data, but the base of a jet provides a natural context for the production of hard X-ray emission like that we have observed.

In Section 3.2, we showed how the data may be fit with a power law modified by reflection; this model is supported by more detailed modeling in Section 3.3. In both of these cases, an incident power law is required; the jet is a natural source of such a power law. In Figure 7, we plot the absorption corrected spectral energy distribution (SED) for *Swift* J1753.5−0127. The optical data are from Zurita et al. (2008) and were taken during at approximately the same time as our *Suzaku* spectra. In addition, we include *V*-band optical and *J*, *H*, and *K*-band NIR data points obtained in April and July 2009 at the Magellan and MDM observatories. The *V*-band magnitude was found to be consistent with the previous measurements of Zurita et al. (2008), as such the NIR data should be representative of the infrared portion of the SED at the time of our *Suzaku* observations. The radio data points represent the radio detection shortly after the 2005 outburst and likely represent upper limits to the radio flux at the time of our observations (Cadolle Bel et al. 2007); these are also consistent with the non-detection at 5 GHz and 8 GHz by Soleri et al. (2008).

The solid line extending from the X-ray to the optical represents a power law as might be expected from optically thin radio emission, i.e., $f_\nu \propto \nu^{-0.5}$. This is similar to the slope of the optically thin jet in GX 339−4 (Corbel & Fender 2002). Extrapolating this power law to optical/NIR wavelengths shows that a spectral break is required at optical/UV frequencies. Analysis of optical data of *Swift* J1753.5−0127 in its current state by Hynes et al. (2009) favors a case where any jet emission is insignificant at optical wavelengths consistent with our extrapolated power-law; this is in agreement with an independent observation/analysis by Durant et al. (2008, 2009). Gandhi (2009) has shown, based on analysis of optical data from XTE J1118+480, GX 339−4, and *Swift* J1753.5−0127 that the variability at optical wavelengths is inconsistent with being produced by reprocessing of X-rays in the accretion disk and instead favor a model where the emission in the LHS is dominated by the jet, e.g., Malzac et al. (2004).

5. CONCLUSIONS

We have presented *Suzaku* broadband X-ray observations of the candidate black hole X-ray binary *Swift* J1753.5−0127. The broadband spectrum (2–250 keV) is observed to be consistent with a simple power-law model ($\Gamma \sim 1.63$). Confirming previous observations, we detect the presence of an excess at soft X-ray energies. In addition, a weak relativistic iron line and curvature consistent with a reflection hump at 20–30 keV are detected.

These observations point toward the persistence of the accretion disk at a much lower radius than previously appreciated in the LHS. Estimates of the disk inner radius with both a simple `diskbb+po` model and a detailed reflection model reveal values consistent with the ISCO ($R_{\rm in} \lesssim 6R_g$) for certain values of both the column density and inclination. In contrast, modeling the spectra with a Comptonization model, while revealing a truncated inner disk ($R_g \sim 50R_g$), implies a value for the Hydrogen column density in disagreement with all previous estimates.

This research has made use of data obtained from the *Suzaku* satellite, a collaborative mission between the space agencies of Japan (JAXA) and the USA (NASA). This research has made use of data obtained from the High Energy Astrophysics Science Archive Research Center (HEASARC), provided by NASA's Goddard Space Flight Center. This research made use of the SIMBAD database, operated at CDS, Strasbourg, France and NASA's Astrophysics Data System.

G.M. thanks the Spanish Ministerio de Ciencia e Innovación and CSIC for support through a Ramón y Cajal contract. J.H. gratefully acknowledges support from NASA grant NNX08AC20G.

REFERENCES

Anders, E., & Grevesse, N. 1989, Geochim. Cosmochim. Acta, 53, 197
Ballantyne, D. R., Iwasawa, K., & Fabian, A. C. 2001, MNRAS, 323, 506
Balucinska-Church, M., & McCammon, D. 1992, ApJ, 400, 699
Beloborodov, A. 1999, ApJ, 510, 123
Burrows, D. N., Racusin, J., Morris, D. C., Roming, P., Chester, M., La Verghetta, R., Markwardt, C. B., & Barthelmy, S. D. 2005, ATel, 547
Caballero Garcia, M. D., et al. 2007, ApJ, 669, 534
Cadolle Bel, M., et al. 2007, ApJ, 659, 549
Corbel, S., & Fender, R. P. 2002, ApJ, 573, 35
D'Angelo, C., Giannios, D., Dullemond, C., & Spruit, H. 2008, A&A, 488, 441
Dickey, J. M., & Lockman, F. J. 1990, ARA&A, 28, 215
Durant, M., Gandhi, P., Shahbaz, T., Fabian, A., Miller, J., Dhillon, V. S., & Marsh, T. R. 2008, ApJ, 682, 45

Durant, M., Gandhi, P., Shahbaz, T., Peralta, H. H., & Dhillon, V. S. 2009, MNRAS, 392, 309
Esin, A., McClintock, J. E., & Narayan, R. 1997, ApJ, 489, 865
Esin, A., Narayan, R., Cui, W., Grove, J. E., & Zhang, S. H. 1998, ApJ, 505, 854
Fender, R. 2006, in Compact Stellar X-ray Sources, ed. W. H. G. Lewin & M. van der Klis (Cambridge: Cambridge Univ. Press)
Fender, R. P., Belloni, T. M., & Gallo, E. 2004, MNRAS, 355, 1105
Fender, R., Garrington, S., & Muxlow, T. 2005, ATel, 558
Fender, R. P., Homan, J., & Belloni, T. M. 2009, MNRAS, 396, 1370
Fukazawa, Y., Mizuno, T., Takahashi, H., Enoto, T., Kokubun, M., Watanabe, S., & the *Suzaku* HXD Team, 2008, JX-ISAS-SUZAKU-MEMO-2008-01
Gallo, E., Fender, R., Kaiser, C., Russell, D., Morganti, R., Oosterloo, T., & Heinz, S. 2005, Nature, 436, 819
Gallo, E., Fender, R. P., & Pooley, G. G. 2003, MNRAS, 344, 60
Gandhi, P. 2009, ApJ, 697, 167
Gierlinski, M., Done, C., & Page, K. 2008, MNRAS, 388, 753
Gierlinski, M., Zdziarski, A. A., Done, C., Johnson, W. N., Ebisawa, K., Ueda, Y., Haardt, F., & Phillips, B. F. 1997, MNRAS, 288, 958
Halpern, J. P. 2005, ATel, 549
Hiemstra, B., Soleri, P., Mendez, M., Belloni, T., Mostafa, R., & Wijnands, R. 2009, MNRAS, 394, 2080
Hynes, R. I., O'Brien, K., Mullally, F., & Ashcraft, T. 2009, MNRAS, 399, 281
Joinet, A., Kalemci, E., & Senziani, F. 2008, ApJ, 679, 655
Kalberla, P. M. W., Burton, W. B., Hartmann, D., Arnal, E. M., Bajaja, E., Morras, R., & Poppel, W. G. L. 2005, A&A, 440, 775
Kokubun, M., et al. 2007, PASJ, 59, 53
Koyama, K., et al. 2007, PASJ, 59, 23
Loar, A. 1991, ApJ, 376, 90
Liu, B. F., Taam, R. F., Meyer-Hofmeister, E., & Meyer, F. 2007, ApJ, 671, 695
Magdziarz, P., & Zdziarski, A. A. 1995, MNRAS, 273, 837
Makishima, K., et al. 2000, ApJ, 535, 632
Makishima, K., et al. 2008, PASJ, 60, 585
Malzac, J., Merloni, A., & Fabian, A. C. 2004, MNRAS, 351, 253
Markoff, S., & Nowak, M. 2004, ApJ, 609, 272
Markoff, S., Nowak, M. A., & Wilms, J. 2005, ApJ, 635, 1203
McClintock, J. E., & Remillard, R. A. 2006, in Compact Stellar X-ray Sources, ed. W. H. G. Lewin & M. van der Klis (Cambridge: Cambridge Univ. Press)
Merloni, A., & Fabian, A. 2002, MNRAS, 332, 165
Merloni, A., Fabian, A. C., & Ross, R. R. 2000, MNRAS, 313, 193
Miller, J. M., Homan, J., & Miniutti, G. 2006a, ApJ, 652, 113
Miller, J. M., Homan, J., Steeghs, D., Rupen, M., Hunstead, R. W., Wijnands, R., Charles, P. A., & Fabian, A. C. 2006b, ApJ, 653, 525
Miller, J. M., et al. 2002, ApJ, 570, 69
Miller, J. M., et al. 2004, ApJ, 606, 131
Miniutti, G., & Fabian, A. C. 2004, MNRAS, 349, 1435
Mitsuda, K., et al. 1984, PASJ, 36, 741
Mitsuda, K., et al. 2007, PASJ, 59, 1
Morgan, E., Swank, J., Markwardt, C., & Gehrels, N. 2005, ATel, 550
Morries, D. C., Burrows, D. N., Racusin, J., Roming, P., Chester, M., La Verghetta, R., Markwardt, C. B., & Barthelmy, S. D. 2005, ATel, 552
Narayan, R., & McClintock, J. E. 2008, New Astron. Rev., 51, 733
Palmer, D. M., Barthelmy, S. D., Cummings, J. R., Gehrels, N., Krimm, H. A., Markwardt, C. B., Sakamoto, T., & Tueller, J. 2005, ATel, 546
Ramadevi, M. C., & Deetha, S. 2007, MNRAS, 378, 182
Reis, R. C., Fabian, A. C., Ross, R. R., & Miller, J. M. 2009, MNRAS, 395, 1257
Ross, R. R., & Fabian, A. C. 1993, MNRAS, 261, 74
Schlegel, D. J., Finkbeiner, D. P., & Davis, M. 1998, ApJ, 500, 525
Serlemitsos, P. J. 2007, PASJ, 59, 9
Shimura, T., & Takahara, F. 1995, ApJ, 445, 780
Soleri, P., et al. 2008, in AIP Conf. Ser. 1010, A Population Explosion: The Nature & Evolution of X-ray Binaries in Diverse Environments, ed. R. M. Bandyopadhyay et al. (San Francisco, CA: ASP), 103
Still, M., Roming, P., Brocksopp, C., & Markwardt, C. B. 2005, ATel, 553
Taam, R. E., Liu, B. F., Meyer, F., & Meyer-Hofmeister, E. 2008, ApJ, 688, 527
Takahashi, T. 2007, PASJ, 59, 35
Takahashi, T., et al. 2008, PASJ, 60, 69
Tomsick, J. A., et al. 2008, ApJ, 680, 593
van der Klis, 2006, in Compact Stellar X-ray Sources, ed. W. H. G. Lewin & M. van der Klis (Cambridge: Cambridge Univ. Press)
Wilkinson, T., & Uttley, P. 2009, MNRAS, 397, 666
Zhang, G. B., Qu, J. L., Zhang, S., Zhang, F., Chen, W., Song, L. M., & Yang, S. P. 2007, ApJ, 659, 1511
Zimmerman, E. R., Narayan, R., McClintock, J. E., & Miller, J. M. 2005, ApJ, 618, 832
Zurita, C., Durant, M., Torres, M. A. P., Shahbaz, T., Casares, J., & Steeghs, D. 2008, ApJ, 681, 1458